ACS EARTH AND SPACE CHEMISTRY

http://pubs.acs.org/journal/aesccq

Article

Ternary Complex Formation of Phosphate with Ca and Mg Ions Binding to Ferrihydrite: Experiments and Mechanisms

Juan C. Mendez* and Tjisse Hiemstra

Cite This: https://dx.doi.org/10.1021/acsearthspacechem.9b00320

Read Online

ACCESS | Metrics & More | Article Recommendations | Supporting Information

ABSTRACT: Calcium (Ca) and magnesium (Mg) are the most abundant alkaline-earth metal ions in nature, and their interaction with ferrihydrite (Fh) affects the geochemical cycling of relevant ions, including phosphate (PO_4). The interfacial interactions of Ca and Mg (M^{2+}) with PO_4 have not been analyzed yet for freshly precipitated Fh. Here, we studied experimentally this interaction in binary M^{2+}-PO_4 systems over a wide range of pH, M^{2+}/PO_4 ratios, and ion loadings. The primary adsorption data were scaled to the surface area of Fh using a recent ion-probing methodology that accounts for the size-dependent chemical composition of this nanomaterial ($FeO_{1.4}(OH)_{0.2}{\cdot}nH_2O$). The results have been interpreted with the charge distribution (CD) model, combined with a state-of-the-art structural surface model for Fh. The CD coefficients have been derived independently using MO/DFT/B3LYP/6-31+G** optimized geometries. M^{2+} and PO_4 mutually enhance their adsorption to Fh. This synergy results from the combined effect of ternary surface complex formation and increased electrostatic interactions. The type of ternary complex formed (anion- *vs* cation-bridged) depends on the relative binding affinities of the co-adsorbing ions. For our Ca-PO_4 systems, modeling suggests the formation of two anion-bridged ternary complexes, i.e., $\equiv(FeO)_2PO_2Ca$ and $\equiv FeOPO_3Ca$. The latter is most prominently present, leading to a relative increase in the fraction of monodentate PO_4 complexes. In Mg-PO_4 systems, only the formation of the ternary $\equiv FeOPO_3Mg$ complex has been resolved. In the absence of Ca, the pH dependency of PO_4 adsorption is stronger for Fh than for goethite, but this difference is largely, although not entirely, compensated in the presence of Ca. This study enables the use of Fh as a proxy for the natural oxide fraction, which will contribute to improved understanding of the mutual interactions of PO_4 and M^{2+} in natural systems.

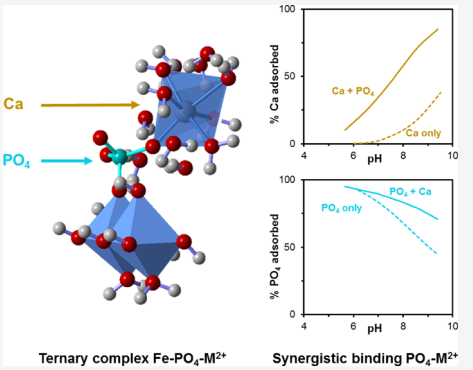

KEYWORDS: *calcium, magnesium, iron oxides nanoparticles, surface complexation modeling, CD model, cooperative and synergistic binding, electrostatic interactions, anion-bridged complexes*

1. INTRODUCTION

Ferrihydrite (Fh) is a nanoparticulate Fe-(hydr)oxide present in almost all natural systems including soils, aquifers, and oceans, and it is also found in mine waste drainage water.[1−3] Due to its relatively low surface energy in comparison to other Fe-(hydr)oxides, Fh is the most thermodynamically stable Fe-(hydr)oxide at a nanosize range of ∼2−8 nm.[4] It is the earliest Fe(III) product that precipitates and works as a precursor of other more crystalline Fe-(hydr)oxides.[5−7] Fh has a high ion adsorption capacity and a large affinity for binding inorganic ions and organic compounds.[8−13] In the environment, the (bio)geochemical cycle of many nutrients and pollutants is largely determined by adsorption processes occurring at the Fh−solution interface.[1] Hence, grasping the interfacial processes of ion binding is essential for understanding the adsorption behavior of ions observed at the macroscopic scale.

A major reason for the extraordinarily high ion adsorption capacity of Fh is its large specific surface area (SSA),[14,15] which, for freshly precipitated Fh, is in the order of ∼600−1100 $m^2\ g^{-1}$.[16] Moreover, Fh has a relatively high surface site density of particularly singly coordinated ($\equiv$FeOH) groups,[17] which are able to bind cations and anions. The singly ($\equiv$FeOH) and triply ($\equiv Fe_3O$) coordinated surface groups of Fh may bind protons, resulting in a pH-dependent net surface charge. The result is an amphoteric behavior of Fh being important for the pH dependency of the adsorption of both metal ions and oxyanions. The mechanisms of ion complexation have been extensively studied for Fh in a long history of *in situ* spectroscopy, quantum chemical computations, and surface complexation modeling, e.g., refs 14 and 18−32. Remarkably, the interaction of Ca and Mg with Fh nanoparticles has received relatively little attention, whereas both elements are highly abundant in the environment and may

Received: December 17, 2019
Revised: March 19, 2020
Accepted: March 25, 2020
Published: March 25, 2020

significantly affect the adsorption of other compounds, particularly oxyanions, such as phosphate (PO_4), arsenate (AsO_4), and selenite (SeO_3).[33−36] In systems with well-crystallized goethite, it has been shown that the adsorption of PO_4 and SeO_3 increases in the presence of, respectively, the alkaline-earth metal ions Ca and Sr.[34,36,37] Qualitatively, similar results have been reported for the adsorption of AsO_4 and PO_4 in the presence of Ca in systems with freeze-dried Fh.[31]

From a quantitative perspective, calcium (Ca^{2+}) is generally the most important metal cation in soil and groundwater.[38] Across different environments, the solution concentration of Ca varies over several orders, being low as $\sim 10^{-5}$ M and high as 10^{-1} M. Magnesium ions (Mg^{2+}) can also be abundant in natural environments. It dominates the composition of divalent cations in marine systems and is important in areas irrigated with Mg-rich water.[36,39] Both alkaline-earth cations (hereinafter jointly referred to as M^{2+}) can specifically adsorb to the surfaces of Fe-(hydr)oxides, affecting the physicochemical properties of the mineral−solution interface and the adsorption of organic and inorganic compounds,[13,33−35] including PO_4.

In aquatic and terrestrial systems, the PO_4 availability is largely controlled by adsorption to the nanosize fraction of Fe and Al-(hydr)oxides[40−42] that can be dissolved in an acid ammonium oxalate solution.[43,44] Thus, Fh can be considered as a relevant model material for studying the mechanisms of PO_4 binding to the natural fraction of metal (hydr)oxides. In most environments, PO_4 ions are simultaneously present with Ca and Mg ions and will interact in combination at the Fh−solution interface. The adsorption of Ca promotes the binding of PO_4 to Fe-(hydr)oxides and *vice versa*.[34,45] This cooperative interaction has been noticed by soil chemists since long ago,[46,47] yet the mechanism of the pH-dependent interplay of PO_4 and Ca^{2+} ions at the surfaces of Fe-(hydr)oxides remains indistinct. However, understanding and quantifying these mutual interactions are highly relevant from a practical perspective of soil chemical analysis. For predicting the availability and mobility of PO_4 in the environment, field samples are often taken and routinely extracted with unbuffered electrolyte solutions.[48,49] These solutions may strongly differ in the concentration of Ca, for instance, soil extractions with 0.01 M $CaCl_2$ solution[50] *vs* soil extractions with demineralized water.[48] The differences in the Ca concentration of the extracting solutions will affect the equilibration of PO_4.[48,51] Translation of these measurements to field conditions not only requires insights into the interfacial interactions of PO_4 and the alkaline-earth metal ions but also their quantification.

Three main mechanisms have been proposed for explaining the synergistic interaction between PO_4 and Ca^{2+} ions at metal-(hydr)oxide surfaces, namely, (i) increase in the interfacial electrostatic interactions; (ii) formation of ternary surface complexes; and (iii) surface precipitation of Ca-PO_4 mineral phases, which may be particularly relevant at high adsorption densities.[28,52−54] Moreover, formation of Fe-PO_4-Ca networks has been reported when Fe(III) coprecipitates in the presence of PO_4 and Ca^{2+} ions.[55] A chemical interaction between Ca and PO_4 is conceivable as these ions can precipitate in a range of minerals whose thermodynamic stability increases at an increase in the Ca/PO_4 ratio.[56] Rationalizing the interfacial interaction between Ca and PO_4 only on the basis of electrostatics has been done for goethite,[34,36] while the additional formation of a ternary Fe-PO_4-Ca complex has been assumed in the case of a freeze-dried Fh material.[31]

For freeze-dried Fh, the cooperative interaction between Ca and PO_4 has been previously investigated.[31] However, the ion adsorption behavior of this material differs from that of freshly prepared Fh because drying leads to irreversible aggregation of the primary particles.[57] This may lead to changes in the crystal morphology, phase transformation of Fh,[58] and undefined reduction of the reactive surface area.[59] Therefore, freshly prepared Fh is chosen in the present study. For this material, we have developed recently a methodology to determine the reactive surface area in a consistent manner with the description of the primary surface charge and specific ion adsorption.[59] For freshly prepared Fh, the cooperative interaction of PO_4 with Ca ions has never been studied nor has it been done for Mg ions. Another advantage of using freshly prepared Fh is the possibility to interpret the collected adsorption data with advanced surface complexation modeling. In addition, we consider freshly prepared Fh as a good proxy for the natural Fe oxide fraction of soils and sediments since Fh particles may precipitate without extensive aggregation if formed in the presence of natural organic matter, which contributes to the thermodynamic stability of Fh and prevents its phase transformation into more stable Fe-(hydr)oxide minerals.[6,60,61]

Based on the above, the objective of the present study is to assess experimentally and by surface complexation modeling the interaction of the alkaline-earth metal ions Ca^{2+} and Mg^{2+} with PO_4 in systems with well-defined, freshly precipitated Fh. In our analysis, we will apply a state-of-art modeling framework that includes recent insights into the surface structure of Fh[26] and the interfacial charge distribution of the complexes formed that will be derived independently from MO/DFT/B3LYP/6-31+G** optimized hydrated clusters. In addition, we will account for the chemical heterogeneity of the reactive sites of Fh for binding divalent metal ions, defining in our modeling sites with high and low affinities for binding Ca^{2+} and Mg^{2+} ions.

For a consistent data interpretation, we will measure the SSA of Fh with a recently developed ion-probing methodology[59] that we will use to scale our primary adsorption data (ion/Fe ratios). In this scaling, we will consistently account for the size dependency of the molar mass of Fh. The latter is due to a particle size-dependent contribution of chemisorbed water (nH_2O), completing the coordination spheres of Fe atoms at the surface of Fh leading to $FeO_{1.4}(OH)_{0.2}{\cdot}nH_2O$.[17] The size-dependent composition also affects the mass density ρ_{nano} (g cm^{-3}) of Fh. This ρ_{nano} will be used to translate the specific surface area into a mean particle diameter that is used to derive the values of the Stern layer capacitances of the compact part of the electrical double layer because this nanomaterial is strongly curved. All the abovementioned factors will be collectively included in the present CD modeling approach together with a recent evaluation of the primary charge of Fh.[59] In our work, we will explore the ternary complex formation, for which will be considering a suite of complexes as candidates to describe our extensive adsorption dataset. Finally, we will address the question of how much Fh differs from well-crystallized goethite in relation to the cooperative binding of Ca-PO_4 and what are the possible implications of using these materials as proxies for the natural oxide fraction.

https://dx.doi.org/10.1021/acsearthspacechem.9b00320
ACS Earth Space Chem. XXXX, XXX, XXX−XXX

2. EXPERIMENTAL SECTION

Ultrapure water (18.2 MΩcm at 25 °C, 1 ppb TOC) and chemical reactants of analytical grade were used to prepare all stock solutions and Fh suspensions. Contact between solutions and air was minimized to avoid the interference of $CO_{2(g)}$ during the adsorption experiments.

2.1. Synthesis of Ferrihydrite. Fh was synthesized according to Hiemstra et al.[16] Briefly, ∼1.0 L of a solution containing ∼3.7 mM $Fe(NO_3)_3{\cdot}9H_2O$ dissolved in 0.01 M HNO_3 was titrated by adding a freshly prepared solution of 0.02 M NaOH. The NaOH solution was initially added at a rate of ∼200 mL min^{-1} until a pH of ∼3.1 was reached. Subsequently, additional base solution was added in ∼5 mL increments until the suspension reached a final pH of ∼8.2. Once the pH was stabilized (∼15 min), the Fh suspension was centrifuged at 3300*g* for 45 min. Next, the supernatant was carefully removed and the settled Fh particles were re-suspended in a solution of 0.01 M $NaNO_3$ to a final volume of typically ∼160 mL. Each freshly prepared Fh suspension was aged for 4 h at 20 °C in closed bottles before starting the adsorption experiments. The total Fe concentration of each Fh suspension was determined in a matrix of 0.8 M H_2SO_4 using ICP-OES. Typically, the total Fe concentration in these suspensions was 20.5 ± 0.5 mM (∼2 g L^{-1}). The specific surface area (m^2 g^{-1}) of each Fh batch was independently measured using surface probing with PO_4.[59] In this approach, the pH-dependent adsorption of PO_4 is measured in single-ion systems. The primary adsorption data (i.e., mol PO_4/mol Fe) are then iteratively interpreted with the CD model, defining the SSA as the only adjustable parameter and accounting for the size dependency of the molar mass (M_{nano}) and mass density (ρ_{nano}) of Fh, as well as the size dependency of the Stern layer capacitance.[59]

2.2. Adsorption Experiments. The adsorption interaction between the alkaline-earth cations (Ca and Mg) and PO_4 was evaluated in binary systems with freshly precipitated Fh. The pH of the adsorption systems ranged between ∼5 and 10, and the background electrolyte concentration was kept constant at 0.01 M $NaNO_3$. Each adsorption system was prepared in 50 mL polypropylene tubes kept under moist-purified N_2(g) to prevent intrusion of CO_2(g) during the preparation of the systems. For the Ca-PO_4 experiments, nine adsorption series were prepared with different molar Ca:PO_4:Fe ratios. Additional series with no Ca addition were prepared and used as a reference for the adsorption of PO_4 in single-ion systems. For the Mg-PO_4 experiments, three adsorption series were prepared at different Mg:PO_4:Fe ratios. Details about the chemical conditions of each adsorption series are presented in Tables S1 and S2 of the Supporting Information. The pH of the adsorption systems was adjusted within the desired range by adding 1.0−2.0 mL of 0.01 M solutions of either HNO_3 or NaOH. Stock solutions of NaH_2PO_4, $Ca(NO_3)_2$, and $Mg(NO_3)_2$ were used to add, respectively, the ions PO_4^{3-}, Ca^{2+}, and Mg^{2+}. To minimize the risk of any precipitation of Ca-PO_4 and Mg-PO_4 solid phases, the systems were pre-equilibrated with PO_4 for 1 h before the corresponding alkaline-earth ion was added. The final volume of each adsorption system was 40.0 mL. All adsorption systems were constantly shaken (120 strokes/min) at 20 °C for 20 h, and next the suspensions were centrifuged at 3330*g* for 20 min to separate the solid and liquid phases. An aliquot of 10 mL was taken from the supernatant of each adsorption system, filtered through a 0.45 μm membrane filter, and acidified with HNO_3 for analysis of the equilibrium concentration of M^{2+} and PO_4. The analysis was done using either ICP-OES or ICP-MS, depending on the final concentrations of the analyzed elements. The settled Fh particles were re-suspended in the 50 mL polypropylene tube to measure the equilibrium pH with a combined glass electrode.

2.3. Modeling. *2.3.1. Charge Distribution (CD) Model.* The results of the M^{2+}-PO_4 adsorption experiments have been interpreted with the charge distribution (CD) model[62] in combination with a recent multisite ion complexation (MUSIC) model for Fh.[26] Details about this structural surface model are described in Section 2.3.2. The electrical double layer (EDL) is described with the extended Stern layer approach.[63] Since Fh is an ultrasmall nanoparticle with a strong surface curvature, the capacitance values ($C_{nano,1}$ and $C_{nano,2}$) of the inner and outer Stern layers are made size-dependent, using well-crystallized goethite as a reference with a near-zero surface curvature.[64] The primary surface charge is described according to Mendez and Hiemstra.[59]

CD modeling was done with ECOSAT version 4.9.[65] The affinity constants (log *K*) of the adsorption reactions of the ternary Fe-PO_4-M^{2+} complexes were optimized using the program FIT version 2.581.[66] The entire set of solution speciation and primary protonation reactions used in the modeling are presented, respectively, in Tables S3 and S4 of the Supporting Information. Software Spartan18 parallel of Wavefunction, Inc. was used to optimize the geometries of the ternary Fe-PO_4-Ca and Fe-PO_4-Mg complexes with molecular orbital (MO) calculations, applying density function theory (DFT). This approach has been also applied to optimize the geometries of the M^{2+}[67] and PO_4[26] complexes adsorbed to Fh. These optimized geometries were interpreted with Brown valence analysis[68,69] to assess the charge distribution of the adsorbed complexes with a small correction for water dipole orientation.[63] The charge attribution to the surface plane (Δz_0) was based on the optimized MO/DFT geometries, whereas the charge distribution over the Stern planes (Δz_1 and Δz_2) was derived for the ternary complexes by fitting to the experimental adsorption data. Details about the template of Fh used in the geometry optimizations are given in Mendez and Hiemstra.[27]

2.3.2. Multisite Ion Complexation Model for Fh. For Fh, a new structural model has been proposed by Michel et al.[70,71] The surface structure has been described by Hiemstra.[17] Since Fh particles are ultrasmall, the surface will dominantly contribute to the overall behavior of this nanomaterial. Many microscopic and macroscopic properties of Fh are size-dependent. A whole suite of physical−chemical properties can be understood from the difference in the polyhedral composition of the mineral core and the surface.[4,17,72,73] With a surface structural analysis of this material, Hiemstra and Zhao[26] have developed a mechanistic multisite ion complexation model for Fh, distinguishing various types of sites and deriving corresponding densities. The model also includes the size-dependent variation of the molar mass (M_{nano}) and the mass density (ρ_{nano}) that results from the variable contribution of chemisorbed water (nH_2O) to the overall chemical composition of Fh ($FeO_{1.4}(OH)_{0.2}{\cdot}nH_2O$).[16]

In the above structural multisite model, three types of surface groups have been defined, which differ in their coordination number with Fe, i.e., singly ($\equiv FeOH^{-0.5}$), doubly ($\equiv Fe_2OH^0$), and triply ($\equiv Fe_3O^{-0.5}$) coordinated

https://dx.doi.org/10.1021/acsearthspacechem.9b00320
ACS Earth Space Chem. XXXX, XXX, XXX−XXX

Table 1. Surface Species, CD Coefficients, and Fitted log *K* for the Binding Reactions of Ca and Mg to Fh Derived in Our Parallel Study[a67]

species	ID[b]	≡FeOH(bl)$^{-0.5}$	FeOH(bh)$^{-0.5}$	Δz_0[c]	Δz_1	Δz_2	H^+	Ca^{2+}	Mg^{2+}	log K ± SE
(≡FeOH)$_2$Ca	BCa(l)	2	0	0.94	1.06	0	0	1	0	2.64 ± 0.03
(≡FeOH)$_2$Ca	BCa(h)	0	2	0.94	1.06	0	0	1	0	5.13 ± 0.02
(≡FeOH)$_2$Mg	BMg(l)	2	0	0.89	1.11	0	0	0	1	1.87 ± 0.06
(≡FeOH)$_2$Mg	BMg(h)	0	2	0.89	1.11	0	0	0	1	4.09 ± 0.04

[a]The surface site densities are from Hiemstra and Zhao[26] with ≡FeOH(a) = 3.0 nm^{-2}, ≡FeOH(b) = 2.8 nm^{-2}, and ≡Fe$_3$O = 1.4 nm^{-2}. Two types of ≡FeOH(b) groups were defined to account for site heterogeneity ≡FeOH(bl) for low affinity and ≡FeOH(bh) for high affinity, having site densities of, respectively, 2.48 ± 0.02 and 0.32 ± 0.02 nm^{-2} for our Fh preparations. The capacitance values for the extended Stern layers of Fh ($C_{nano,1}$ and $C_{nano,2}$) are size-dependent[59] (see Tables S1 and S2) and were calculated by taking as a reference the capacitance values of goethite (C_1 = 0.90 F m^{-2} and C_2 = 0.74 F m^{-2}) [b]BCa(l) = bidentate (double-corner) Ca with low affinity sites; BCa(h) = bidentate (double-corner) Ca with high affinity sites; BMg(l) = bidentate (double-corner) Mg with low affinity sites; BMg(h) = bidentate (double-corner) Mg with high affinity sites [c]The CD coefficients have been derived from MO/DFT optimized geometries.

Table 2. Surface Species, CD Coefficients, and Fitted log *K* for the Formation of Ternary Complexes in the Binary Systems PO$_4$-Ca (R^2 = 0.99 and n = 72) and PO$_4$-Mg (R^2 = 0.99 and n = 22) with Fh[a]

species	ID	≡FeOH(a)[b]	≡FeOH(bl)[d]	FeOH(bh)[b]	Δz_0	Δz_1	Δz_2	H^+	M^{2+}	PO_4^{-3}	log K ± SE[c]
≡FeOPO$_3$Ca[d]	MPCa(a)	1	0	0	0.24	−1.30	1.06	1	1	1	22.27 ± 0.12
≡FeOPO$_3$Ca[d]	MPCa(bl)	0	1	0	0.24	−1.30	1.06	1	1	1	22.27 ± 0.12
≡FeOPO$_3$Ca[d]	MPCa(bh)	0	0	1	0.24	−1.30	1.06	1	1	1	22.27 ± 0.12
≡(FeO)$_2$PO$_2$Ca[e]	BPCa(bl)	0	2	0	0.62	−1.08	1.46	2	1	1	30.09 ± 0.12
≡(FeO)$_2$PO$_2$Ca[e]	BPCa(bh)	0	0	2	0.62	−1.08	1.46	2	1	1	30.09 ± 0.12
≡FeOPO$_3$Mg[d]	MPMg(a)	1	0	0	0.22	−1.55	1.33	1	1	1	22.00 ± 0.10
≡FeOPO$_3$Mg[d]	MPMg(bl)	0	1	0	0.22	−1.55	1.33	1	1	1	22.00 ± 0.10
≡FeOPO$_3$Mg[d]	MPMg(bh)	0	0	1	0.22	−1.55	1.33	1	1	1	22.00 ± 0.10

[a]The surface site densities are from Hiemstra and Zhao[26] with ≡FeOH(a) = 3 nm^{-2}, ≡FeOH(b) = 2.8 nm^{-2}, and ≡Fe$_3$O = 1.4 nm^{-2}. Two types of ≡FeOH(b) groups were defined to account for the surface site heterogeneity of the adsorption of M^{2+} (≡FeOH(bl) and ≡FeOH(bh) for low and high affinities, respectively). [b]≡FeOH(a)$^{-0.5}$ with PO$_4$ forms only monodentate complexes, whereas ≡FeOH(b)$^{-0.5}$ forms both mono- and bidentate (double corner) complexes (see section 2.3.2). [c]log K values derived in this study by fitting of the experimental data obtained in the binary Ca-PO$_4$ and Mg-PO$_4$ systems. [d]Δz_2 = 1.06 v.u. (± 0.06) can be explained as the Ca complexation to adsorbed PO$_4$ in ≡FeOPO$_3$-Ca-(OH$_2$)$_n$ with remaining charge attribution of Ca to three OH$_2$ ligands in the outer Stern plane. For the ternary complexes MPMg, a higher Δz_2 value of 1.33 v.u. (± 0.07) suggest that Mg is more loosely bound to PO$_4$ than Ca (see text). [e]Δz_2 = 1.46 v.u. (± 0.17) can be explained as the Ca complexation to adsorbed PO$_4$ in ≡(FeO)$_2$PO$_2$-Ca-(OH$_2$)$_n$ with a charge attribution of Ca to four OH$_2$ ligands in the outer Stern plane.

groups. Structurally, two types of singly coordinated groups can be distinguished, i.e., ≡FeOH(a)$^{-0.5}$ and ≡FeOH(b)$^{-0.5}$, which may form, respectively, either single-edge (^{1}E) or double-corner (^{2}C) bidentate surface complexes having, respectively, a surface density of N_s(a) = 3.0 ± 0.6 nm^{-2} and N_s(b) = 2.8 ± 0.6 nm^{-2}. Both types of singly coordinated groups may also form single-corner (^{1}C) monodentate surface complexes. The triply coordinated groups do not participate in ligand exchange reactions, but they contribute to the development of the primary surface charge. At the surfaces of Fh, different types of triply coordinated groups are found with a large variation in their proton affinity (log K_H). The surface charge introduced by groups with a low log K_H (≡Fe$_3$O$^{-0.5}$) is compensated by groups with a high log K_H (≡Fe$_3$OH$^{+0.5}$), leading to an effective site density of $N_{s,(T)}$ = 1.4 ± 0.5 nm^{-2}, if the charging behavior of these triply coordinated groups is represented by an equivalent surface site with a log K_H = ∼8.1, as for the singly coordinated groups.[26] The ≡Fe$_2$OH^0 groups are presumably uncharged and do not react with protons under common pH conditions. This model has been applied to describe consistently the primary surface charge[59] and the adsorption of a range of oxyanions, such as PO$_4$, AsO$_4$, As(OH)$_3$,[26] Si(OH)$_4$,[72] and CO$_3$,[27] as well as the adsorption of a series of alkaline-earth metal cations.[67]

2.3.3. Description of Ion Adsorption in Single Systems. In a parallel study, we have shown that the CD model can describe very well the adsorption of Ca^{2+} and Mg^{2+} (M^{2+}) to Fh in single-ion systems over a broad range of solution conditions, comprising different initial M^{2+} concentrations and molar M^{2+}/Fe ratios, as well as pH and ionic strength levels.[67] The data can be described by defining in the modeling the formation of a binuclear bidentate complex according to

$$2 \equiv \mathrm{FeOH(b)}^{-0.5} + \mathrm{M}^{2+} \leftrightarrow \equiv(\mathrm{FeOH(b)})_2^{-1+\Delta z0}\mathrm{M}^{\Delta z1} \quad \log K_{BM} \qquad (1)$$

where Δz_0 and Δz_1 are the CD coefficients derived from the Brown bond valence analysis applied to the MO/DFT optimized geometries (Table 1). Bidentate complex formation is supported by our combined interpretation of MO/DFT geometry optimizations[67] and EXAFS data for the adsorption of divalent cation to Fe (hydr)oxides.[25,37,74−76] This binding mechanism is also supported by the thermodynamic analysis of macroscopic data such as the H^+/M^{2+} exchange ratio reported for Ca[77] and the marked pH dependency of Ca adsorption observed in our adsorption experiments.

In that same parallel study, we have also shown that the adsorption sites of Fh for binding M^{2+} exhibit chemical heterogeneity, which is a common reported phenomenon for the binding of metal ions to Fh.[14,20,78] The high affinity sites dominate the adsorption at low M^{2+} concentrations, and for our Fh preparation, these surface sites have a density of N_s(bh) = 0.32 ± 0.02 nm^{-2}. The corresponding site density for the low

https://dx.doi.org/10.1021/acsearthspacechem.9b00320
ACS Earth Space Chem. XXXX, XXX, XXX−XXX

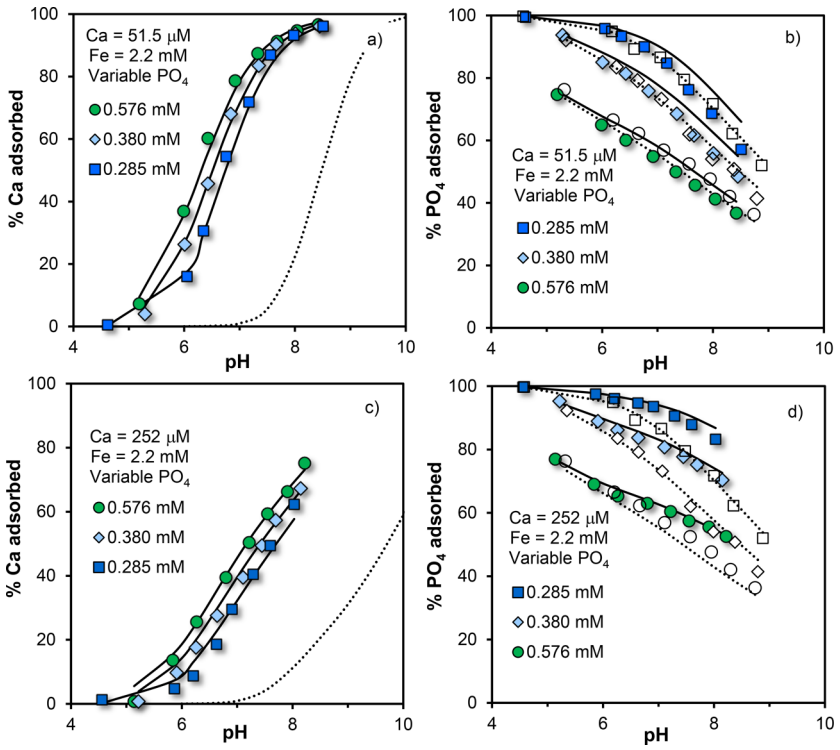

Figure 1. pH-dependent adsorption of Ca (left panels) and PO_4 (right panels) in binary ion systems with Fh. The ionic strength was kept constant at I = 0.01 M $NaNO_3$, and the specific surface area of this Fh suspension was A = 684 ± 15 m^2 g^{-1} with a corresponding molar mass of M_{nano} = 96.6 g mol^{-1} Fe. The symbols are the experimental data, and the lines are the CD model calculations obtained with the parameter sets of Tables 1 and 2. The adsorption parameters of PO_4 in single-ion systems are taken from Hiemstra and Zhao.[26] The total concentrations of Fe, Ca, and PO_4 are given in each panel. The initial Ca loadings in systems a, b and c, d are equivalent to, respectively, ∼0.4 and ∼1.7 μmol m^{-2}, and the equivalent initial PO_4 loadings vary from ∼2.0 to 3.9 μmol m^{-2}. For comparison, model predictions are given for the corresponding single-ion systems, i.e., without addition of either Ca or PO_4 (dotted lines). For PO_4, the adsorption in single-ion systems was additionally measured for each experimental condition (open symbols). The adsorption of Ca and PO_4 is promoted in the binary systems by mutual electrostatic interactions and the formation of ternary PO_4-Ca surface complexes.

affinity sites can be set to N_s(bl) = 2.48 nm^{-2}, as the sum of both types of FeOH(b) $^{-0.5}$ groups is 2.8 nm^{-2}.[26]

For describing the adsorption of PO_4 in single-ion systems, we have used the set of CD model parameters derived by Hiemstra and Zhao.[26] For the adsorption of oxyanions that strongly interact with Fh such as PO_4, we do not experience explicitly in our modeling the presence of high affinity sites, in line with previous suggestions given by Dzombak and Morel.[14] Probably, the high affinity character of these sites is masked by the already rather large PO_4 loading of the low affinity sites. Therefore, we have used in our modeling the same set of log K values for PO_4 binding to both types of $FeOH(b)^{-0.5}$ groups (Table 2 and Table S4).

3. RESULTS AND DISCUSSION

3.1. Interaction of Calcium and Magnesium with Phosphate: Experimental Results. The interaction of the alkaline-earth metal Ca with PO_4 in Fh systems has been studied extensively in the present work. In Figures 1 and 2, the left panels show the adsorption edges of Ca to Fh in the binary Ca-PO_4 systems, whereas the right panels show the corresponding PO_4 adsorption data. In Figure 1, the upper panels are for a total Ca concentration of ∼0.05 mM, and the lower panels are for systems with a 5-fold higher concentration of added Ca (∼0.25 mM). In Figure 2, we give the adsorption data for binary Ca-PO_4 systems with a higher Fh concentration. This allows an accurate measurement of the adsorption of Ca to Fh at higher total added Ca concentrations, i.e., ∼1.0 mM (upper panels) and ∼0.62 mM (lower panels). For comparison, we also present in Figures 1 and 2 the model predictions (dotted lines) and/or the measured adsorption data (open symbols) of the corresponding single-ion systems at the same initial ion loading.

At a given pH, the adsorption of Ca to Fh increases simultaneously with an increase in the initial concentration of PO_4. In comparison to the single-ion systems, the adsorption edges of Ca are significantly shifted toward lower pH values (∼2.0 pH units) in the presence of PO_4. For systems with the same total Fe content, this shift of the adsorption edges is more pronounced for systems with lower total molar Ca/PO_4 ratios. Simultaneously, the adsorption of PO_4 to Fh increases in the presence of Ca, but the synergistic effect of Ca on the PO_4 adsorption is less pronounced than the corresponding effect of PO_4 on the adsorption of Ca.

The cooperative interaction of ions adsorbed to Fh was also evaluated in the binary Mg-PO_4 systems. Figure 3a,c shows that in the presence of PO_4, the adsorption edges of Mg are shifted toward lower pH values (closed symbols), in comparison to the adsorption of Mg in the single-ion systems (open symbols). In Figure 3b, the adsorption of PO_4 in the absence (open symbols) and presence (closed symbols) of Mg is compared for Fh systems with two different values for the total molar Mg/PO_4 ratios: 0.5 (circles) and 0.05 (squares). The percentage of PO_4 adsorbed increases in the presence of Mg. Additionally, the pH dependency of the PO_4 adsorption is

https://dx.doi.org/10.1021/acsearthspacechem.9b00320
ACS Earth Space Chem. XXXX, XXX, XXX−XXX

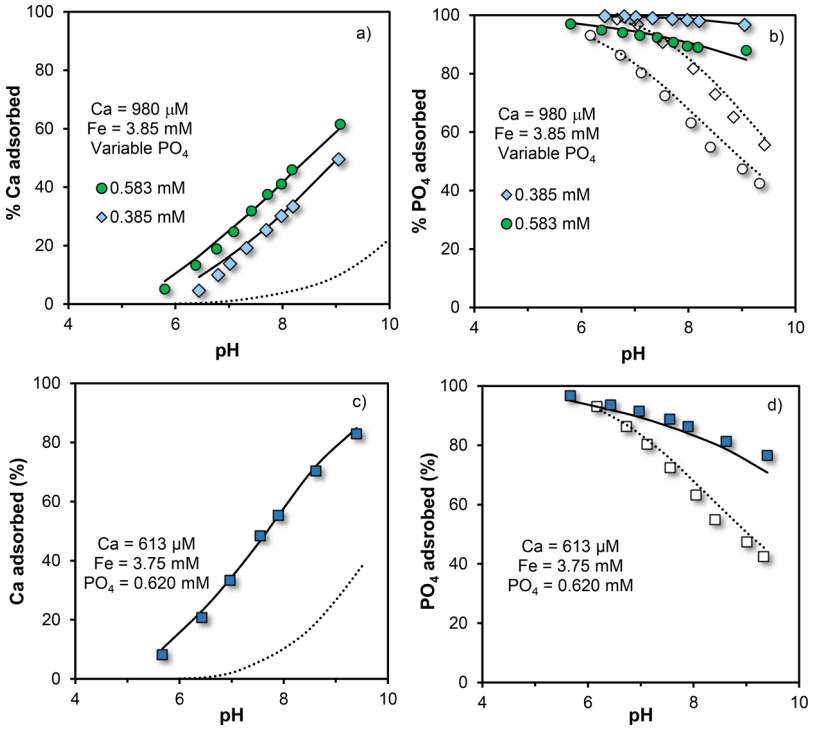

Figure 2. pH-dependent adsorption of Ca (left panels) and PO_4 (right panels) in single- and binary ion systems with Fh in I = 0.01 M $NaNO_3$. The specific surface area of this Fh suspension was A = 684 ± 15 m^2 g^{-1} with a corresponding molar mass of M_{nano} = 96.6 g mol^{-1} Fe. The total concentrations of Fe, Ca, and PO_4 are given in each panel. The initial loadings of Ca in systems a, b and c, d are equivalent to, respectively, ∼3.9 and ∼2.5 μmol m^{-2}. The initial PO_4 loadings are equivalent to ∼1.5−2.3 μmol m^{-2} in systems a, b and ∼2.5 in systems c, d. The closed symbols and the full lines are, respectively, experimental data and CD model calculations for binary systems. For comparison, the model predictions are given for single-ion systems, i.e., without addition of either Ca or PO_4 (dotted lines). For PO_4, the adsorption in single-ion systems was also measured for each experimental condition (open symbols). The CD model parameter sets are given in Tables 1 and 2. The adsorption parameters of PO_4 in single-ion systems are taken from Hiemstra and Zhao.[26] The capacitance values are given in Table S1.

strongly reduced in the systems with a relatively high molar Mg/PO_4 ratio, e.g., ∼1.6 (Figure 3d).

The model lines in Figures 1−3 show the capability of the CD model to describe accurately the interfacial interactions of the alkaline-earth metal ions Ca and Mg with PO_4 over a wide range of conditions in the Fh systems. Synergy between these cations and PO_4 has been also reported for freeze-dried Fh,[31] goethite (α-FeOOH),[34−36] hydrous zirconium oxide (HZO),[79] and manganese dioxide (δ-MnO_2).[80] However, the dominant mechanisms explaining these interactions might differ between these oxide materials. For Fh, details about the mechanisms of synergetic binding will be discussed in the next section.

3.2. Modeling and Mechanisms of M^{2+}-PO_4 Adsorption Synergy. *3.2.1. Effect of Electrostatic Interactions.* The adsorption of M^{2+} is significantly promoted by PO_4 in all binary systems in comparison to the corresponding single-ion systems (dotted lines and/or open symbols in the left panels of Figures 1−3). In contrast, the PO_4 adsorption in the binary systems (right panels in Figures 1−3) increases mainly at high pH and high initial M^{2+} concentration due to the presence of M^{2+}. The reason for this difference is the higher affinity of PO_4 for the adsorption to Fh, in comparison with the adsorption affinity of M^{2+}. The large quantities of adsorbed PO_4 can change substantially the net particle charge of Fh, whereas the presence of M^{2+} in the binary systems affects notably less the net particle charge, as it can be shown by modeling.

In the absence of specific ion adsorption, the point of zero charge of Fh in $NaNO_3$ solutions is pH_{PZC} ≈ 8.1.[59] Our CD modeling shows that the adsorption of PO_4 to Fh provokes a decrease in the isoelectric point (IEP) to pH_{IEP} ≈ 4.5−5.0 (Figure S1a). It implies that, under these conditions, a negative double layer potential (ψ) is created in a major part of the pH range of our study. This induces a shift of the adsorption edges of Ca^{2+} and Mg^{2+} in the presence of PO_4 (Figures 1−3) and stimulates the formation of ternary surface species (Section 3.2.2). The binding of Ca^{2+} or Mg^{2+} ions in the binary systems with PO_4 partly compensates the negative charge created by the adsorbed PO_4 ions, and in turn, this promotes the adsorption of PO_4 in the binary systems, particularly at high pH. It can be shown that at a sufficiently high Ca concentration, binary Ca-PO_4 systems with Fh may have two pH values where the particle charge switches, i.e., two pH_{IEP} values, one at low pH and one at high pH (Figure S1b).

Figure 4 presents the concentrations of Ca (panel a) and PO_4 (panel b) in the equilibrium solution of the respective single- (open symbols) and binary (closed symbols) Fh systems. The experimental data of the binary systems cannot be explained by using only the adsorption reactions found for the single-ion systems (dotted lines) in the modeling. Figure 4 illustrates that mutual electrostatic interactions alone are not enough to explain the adsorption data in binary Ca-PO_4 systems. This finding contrasts with that in goethite systems, in which the cooperative binding of Ca^{2+} and Mg^{2+} ions with PO_4 could be well predicted assuming only electrostatic interactions.[34−36] Differences in the adsorption interaction of Ca-PO_4 between Fh and goethite are discussed in Section 3.4. In our Fh systems, the precipitation of a calcium phosphate

https://dx.doi.org/10.1021/acsearthspacechem.9b00320
ACS Earth Space Chem. XXXX, XXX, XXX−XXX

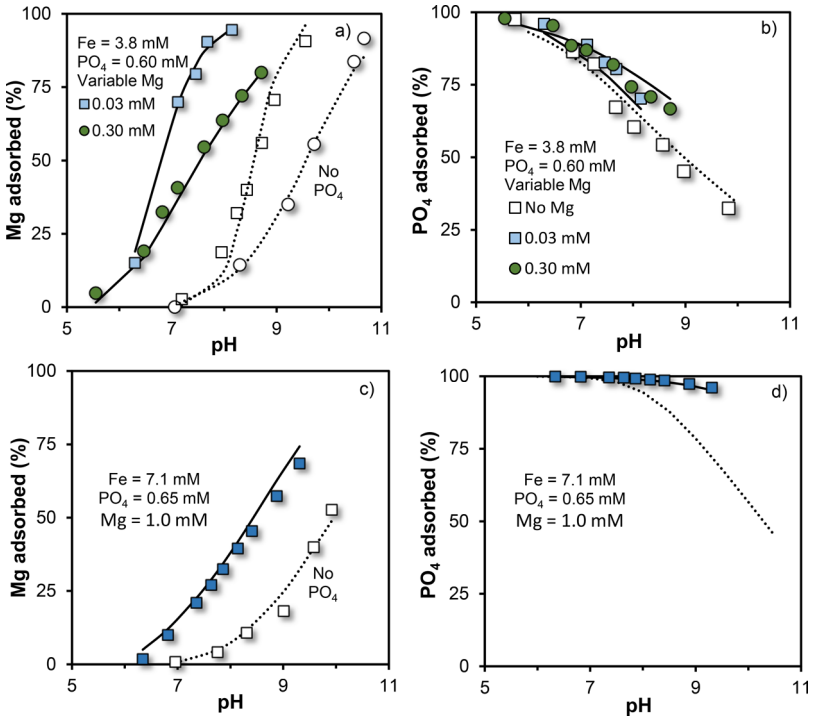

Figure 3. pH-dependent adsorption of (a, c) Mg and (b, d) PO_4 in single- (open symbols) and binary (closed symbols) ion systems with Fh in I = 0.01 M $NaNO_3$. The specific surface area of this Fh suspension was $A = 720 \pm 10$ m^2 g^{-1} with a corresponding molar mass of M_{nano} = 97.6 g mol^{-1} Fe. The symbols are the experimental data, and the lines are the CD model results obtained with the parameter sets of Tables 1 and 2. The adsorption parameters of PO_4 in single-ion systems are taken from Hiemstra and Zhao.[26] The total concentrations of Fe, Mg, and PO_4 are given in each panel. The initial loadings of Mg are equivalent to ~0.1 and ~1.1 μmol m^{-2} in systems a, b and ~2.0 μmol m^{-2} in systems c, d. The initial PO_4 loadings are equivalent to, respectively, ~2.2 and 1.3 μmol m^{-2} in systems a, b and c, d. For comparison, the respective adsorption series in single-ion systems have been measured (open symbols) and/or modeled (dotted line). The capacitance values are given in Table S2.

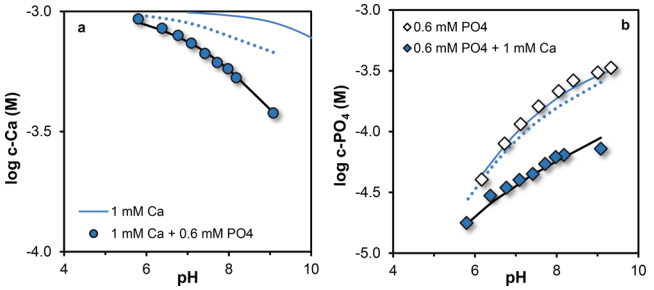

Figure 4. Logarithm of the (a) Ca and (b) PO_4 concentrations in the equilibrium solution of systems with Fh in I = 0.01 M $NaNO_3$. The total Fe concentration was 3.9 mM, and the specific surface area of this Fh suspension was $A = 684 \pm 15$ m^2g^{-1} with a respective molar mass M_{nano} = 96.6 g mol^{-1} Fe. Closed symbols are for the binary Ca-PO_4 systems with total concentrations of Ca = 1.0 mM and PO_4 = 0.6 mM, and the open symbols are for the single-ion systems. The dotted lines are the CD model predictions using only the adsorption parameters of the single-ion systems of Ca (Table 1) and PO_4,[26] whereas the full lines are the modeling results including for the binary systems the formation of ternary surface complexes (Table 2).

mineral cannot explain the significant reduction of concentrations in the Ca and PO_4 systems neither, as illustrated in Section 4 of the Supporting Information. For the Mg-PO_4 systems, the same results are observed (Figure S4).

3.2.2. Formation of Ternary Ca-PO_4 Surface Complexes. The adsorption data of Ca and PO_4 in the binary systems can only be described by including in the modeling the formation of ternary surface complexes. In general, Ca and PO_4 have contrasting affinities for binding to metal (hydr)oxides. Ca^{2+} ions have a much lower intrinsic affinity than PO_4 ions for the binding sites at the surface of Fh. However, Ca^{2+} ions do have a high affinity for PO_4, which is reflected by the increasing stability of Ca-PO_4 minerals at increasing molar Ca/PO_4 ratio of these minerals.[56] In the case of ternary complex formation, it is therefore more likely that Ca will bind to adsorbed PO_4 rather than the opposite. This idea is supported by literature data of Fe-PO_4-Ca co-precipitation showing direct complexation of PO_4 to Fe(III) polymers, where these units form larger networks that are interconnected by Ca^{2+} ions.[55,81] High-energy X-ray scattering with pair distribution function analysis showed double-corner $\equiv(FeO)_2PO_2$ complexes linked together by Ca ions bound as single-corner complexes[55] with a Ca-P distance of 360 pm. *In situ* spectroscopic studies have also suggested the formation of PO_4-bridged ternary complexes with Ca in adsorption systems with hydrous zirconium oxide[79] and titanium dioxide (TiO_2).[82]

The binding of Ca^{2+} cations to already adsorbed PO_4 anions (i.e., formation of anion-bridged ternary complexes) is also supported by the modeling of the Ca and PO_4 adsorption data of our binary Ca-PO_4 systems with Fh (Figures 1 and 2). Our extensive modeling of these systems shows that the use of cation-bridged ternary complexes (i.e., Fe-Ca-PO_4) did not provide a good description of the adsorption of both Ca and PO_4 in the binary systems. Instead, our modeling advocates the formation of anion-bridged complexes, in which the Ca^{2+} ion is located at a larger distance from the surface.

The formation reactions of the ternary complexes ultimately derived after extensive modeling are

https://dx.doi.org/10.1021/acsearthspacechem.9b00320
ACS Earth Space Chem. XXXX, XXX, XXX−XXX

$$\equiv \mathrm{FeOH}^{-0.5} + \mathrm{H}^{+}(\mathrm{aq}) + \mathrm{PO_4}^{3-}(\mathrm{aq}) + \mathrm{Ca}^{2+}(\mathrm{aq}) \quad \log K_{\mathrm{MTC}}$$
$$\leftrightarrow \equiv \mathrm{FeO}^{-0.5+\Delta z0}\mathrm{PO_3}^{\Delta z1}\mathrm{Ca}^{\Delta z2} + \mathrm{H_2O(l)} \quad (2)$$

$$2 \equiv \mathrm{FeOH}^{-0.5} + 2\,\mathrm{H}^{+}(\mathrm{aq}) + \mathrm{PO_4}^{3-}(\mathrm{aq}) + \mathrm{Ca}^{2+}(\mathrm{aq}) \quad \log K_{\mathrm{BTC}}$$
$$\leftrightarrow \equiv (\mathrm{FeO})_2^{-1+\Delta z0}\mathrm{PO_2}^{\Delta z1}\mathrm{Ca}^{\Delta z2} + 2\,\mathrm{H_2O(l)} \quad (3)$$

where Δz_0, Δz_1, and Δz_2 are the CD coefficients of the 0-, 1-, and 2-plane in the extended Stern layer model. The corresponding set of adsorption parameters is given in Table 2.

For both the above surface complexes, the values of Δz_0 have been derived with the Brown bond valence analysis[68,69] of the optimized geometries of these ternary complexes that we obtained with MO/DFT/B3LYP/6-31+G** calculations (Section 5 in the Supporting Information), whereas the values of Δz_1 and Δz_2 were adjusted by fitting the model to the adsorption data using the constraint $\Delta z_{tot} = \Delta z_0 + \Delta z_1 + \Delta z_2$. The optimized MO/DFT structures of the ternary complexes defined with eqs 2 and 3 are represented in Figure 5a,b,

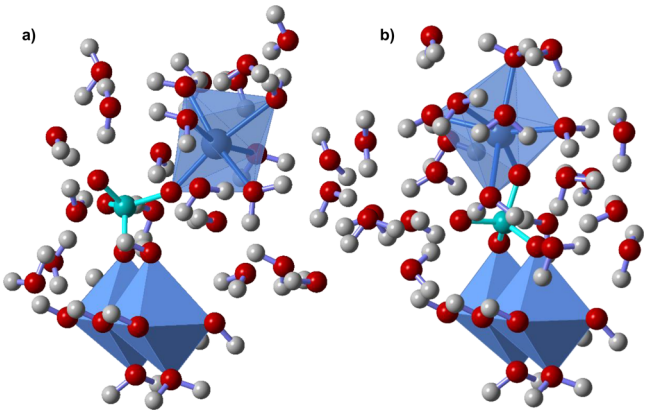

Figure 5. Hydrated geometries of the ternary Fe-PO_4-Ca complexes optimized with MO/DFT/B3LYP/6-31+G**. (a) Single-corner complex of $\equiv$FeOPO$_3$ (d(Fe-P) = 348 pm) with a Ca ion that is bound to PO_4 as a Ca-O-P single-corner (^{1}C) complex (d(P-Ca) = 367 pm), formed according to eq 2. (b) Double-corner complex of $\equiv(\mathrm{FeO})_2\mathrm{PO_2}$ (d(Fe-P) = 320 ± 4 pm) with a Ca ion that is bound to PO_4 as a Ca-O-P single-corner (^{1}C) complex (d(P-Ca) = 327 pm), formed according to eq 3. The $\mathrm{Fe_2(OH)_6(OH_2)_3PO_4}$-Ca cluster (a) has 26 water molecules for hydration and the other one (b) has 21.

respectively. Both the mononuclear monodentate $\equiv$FeOPO$_3$ complex (Figure 5a) and the binuclear bidentate $\equiv(\mathrm{FeO})_2\mathrm{PO_2}$ complex (Figure 5b) interact with Ca by forming one single Ca-O-P bond. In the former complex, the calculated Ca-P distance was 367 pm, and in the latter, it was 327 pm. In a hydrated calcium phosphate mineral, brushite ($\mathrm{CaHPO_4{\cdot}2H_2O}$), a Ca-P distance of 370 ± 2 pm can be found in the case of single Ca-O-P bridging, which is close to the distance (360 pm) observed in $\equiv(\mathrm{FeO})_2\mathrm{PO_2Ca}$ networks[55] and found also in hydroxyapatite. In brushite, a shorter Ca-P distance of 312 pm is also found for single Ca-O-P linkages.

The ternary complex in which PO_4 is bound to Fh in a monodentate configuration (MPCa) (eq 2) is the most relevant ternary surface species for describing our experimental data of the binary Ca-PO_4 systems (see below Figure 6). This complex can be formed with both types of singly coordinated

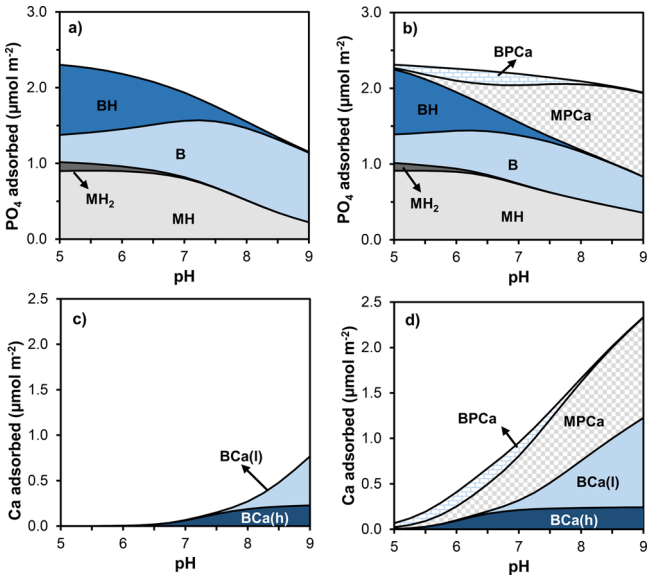

Figure 6. pH-dependent surface speciation of PO_4 (upper panels) and Ca (lower panels) in the corresponding single-ion (left panels) and binary Ca–PO_4 (right panels) systems with Fh in 0.01 M $NaNO_3$. The conditions of the systems are similar to those of the adsorption experiments shown in Figure 2a,b and Figure 4. The total Fe concentration is 3.90 mM, and the specific surface area of Fh is A = 684 m^2 g^{-1} with a corresponding molar mass of M_{nano} = 96.6 g mol^{-1}. The total PO_4 and Ca concentrations are, respectively, 0.60 mM and 1.0 mM. For PO_4: MH = monodentate protonated; MH_2 = monodentate doubly protonated; B = bidentate; BH = bidentate protonated. For Ca: BCa(l) = bidentate at the low affinity sites; BCa(h) = bidentate at the high affinity sites. For the ternary species: MPCa = ternary complex in which PO_4 is bound as a monodentate; BPCa = ternary complex in which PO_4 is bound as a bidentate. The calculations have been done using the CD model with the parameter sets of Tables 1, 2 and Table S4 in the Supporting Information.

groups $\equiv$FeOH(a)$^{-0.5}$ and $\equiv$FeOH(b)$^{-0.5}$. A similar type of complex was used by Antelo et al.[31] for describing Ca-PO_4 binary systems with freeze-dried Fh. However, their data set covers a relatively small range of solution conditions compared to our work, in which we collected adsorption data at a wider range of Ca/Fe ratios. This allows us to reveal by modeling the formation of an additional ternary complex (BPCa), in which Ca is bound to an adsorbed PO_4 present in the bidentate configuration (eq 3). Moreover, in our modeling, we have implemented the difference in high and low affinity sites for Ca, enabling a good description of the Ca binding over a wide range of Ca loadings. With the two ternary complexes resolved, an excellent and consistent description of the simultaneous adsorption of Ca and PO_4 is possible (R^2 = 0.99 and n = 72), as shown in Figures 1 and 2 with the modeled lines.

For the binary Mg-PO_4 systems, only the formation of one ternary complex is required for describing adequately the interaction of these two ions with the surfaces of Fh (R^2 = 0.99 and n = 22). In this ternary complex, PO_4 is bound to Fh in a monodentate configuration (MPMg), similar to that for the ternary Fe-PO_4-Ca complex formulated in eq 2. The respective adsorption reaction is formulated as

https://dx.doi.org/10.1021/acsearthspacechem.9b00320
ACS Earth Space Chem. XXXX, XXX, XXX−XXX

$$\equiv FeOH^{-0.5} + H^{+}(aq) + PO_4^{3-}(aq) + Mg^{2+}(aq) \quad \log K_{MTC} \leftrightarrow \equiv FeO^{-0.5+\Delta z0}PO_3^{\Delta z1}Mg^{\Delta z2} + H_2O(l) \tag{4}$$

Presently, we have not been able to clearly reveal the formation of the ternary Fe-PO_4-Mg complex, in which PO_4 is bound to Fh in a bidentate configuration (BPMg), as we did resolve for the Ca-PO_4 systems. Introduction of such BPMg does not improve the description of our adsorption data in the Mg-PO_4 systems, and a large uncertainty is found in the fitting of the CD coefficients of the 1- and 2-planes (i.e., Δz_1 and Δz_2) of this ternary species. It must be noticed that for the Mg-PO_4 systems, we have collected a more limited dataset, covering a narrower range of solution conditions in comparison to the Ca-PO_4 systems. This may have affected the resolution of our modeling approach to distinguish the potential formation of an additional ternary complex species. Considering this constraint, we have implemented in our final modeling only the formation of the ternary complex MPMg.

In the series of alkaline-earth metal ions, Ca^{2+} interacts stronger than Mg^{2+} with Fh, which is reflected in its higher log K values ($\Delta \log K \approx 0.9$) for high and low affinity sites (Table 1). This difference in log K might be attributed to an exchange of interfacial water, releasing Gibbs free energy.[67] For the formation of monodentate ternary complexes (eq 2 and 4), we find a difference in affinity of $\Delta \log K_{MTC} \approx 0.3$ between the ternary complexes with Ca and Mg, which is possibly also due to an exchange of interfacial water because, in solution, both association constants ($CaHPO_4^0(aq)$ and $MgHPO_4^0(aq)$) are rather similar.[83] The stronger interaction of Ca with PO_4 at the surface of Fh can be also inferred from our MO/DFT calculations. Ca^{2+} neutralizes the negative charge of PO_4 ligands better than Mg^{2+}, which leads to lower attribution of the negative charge of PO_4 to the surface and, consequently, to slightly higher Δz_0 values for the MPCa complex. In addition, the fitted Δz_2 value is higher for the MPMg than for the MPCa complex (Table 2), suggesting that a higher fraction of Mg charge is located in the outer Stern layer region. Overall, these results suggest that Mg is more loosely bound to PO_4 than Ca at the surfaces of Fh. In Figure S6 of the Supporting Information, we modeled the PO_4 binding to Fh in the presence of either Ca or Mg. At the same solution conditions (i.e., pH and total M^{2+} concentration), the adsorption of PO_4 is more enhanced in the presence of Ca in comparison to Mg.

In literature, formation of both anion-bridged (e.g., Fe-PO_4-M^{2+}) and metal-bridged (e.g., Fe-M^{2+}-PO_4) ternary complexes have been proposed.[53] In general, the type of ternary complexes formed would depend on the relative affinity of the co-adsorbing ions for the Fe-(hydr)oxide surfaces.[53] If the anion interaction with the surface is relatively weak, metal-bridged ternary complexes dominate, as found, for instance, in Cd-SO_4 and Pb-SO_4 systems.[28,84,85] In our case, the anion (PO_4^{3-}) is much stronger bound to Fh than the cation (Ca^{2+} or Mg^{2+}) and this leads to the formation of anion-bridged complexes.

In specific cases, it is also possible that both cations and anions react directly with the surfaces,[25,28,53] as found in Pb-PO_4 systems.[86] In that type of complex, both ions are bound to the surface in a monodentate manner, but there is an additional chemical (lateral) interaction between the adsorbed cation and anion.[53] Conceptually, all charges are then located in the inner Stern layer region (0- and 1-plane). When a ternary anion-bridged surface complex is formed, part of the complex (M^{2+}) may physically enter the outer Stern layer region (2-plane). This is found with our CD modeling for the $\equiv(FeO)_2PO_2$-Ca and $\equiv FeOPO_3$-Ca complexes. According to the CD model, ~two/thirds of the Ca charge in the $\equiv(FeO)_2PO_2$-Ca complex is at the 2-plane ($\Delta z_2 = +1.46 \pm 0.17$ v.u.), which could suggest that ~two/thirds of the Ca ligands are in the outer Stern layer. This attribution of positive charges of the ternary Fe-PO_4-Ca complexes to the 2-plane will have important implications for describing the pH-dependent PO_4 adsorption in Ca media, as it will be discussed in Section 3.4.

3.3. Surface Speciation: Single- *vs* Binary Ion Systems. In Figure 6, the surface speciation of PO_4 and Ca in single-ion systems (left panels) is compared to the corresponding surface speciation of these ions in the binary Ca-PO_4 systems (right panels). The calculations have been done with the CD model and the simulated conditions of the binary Ca-PO_4 systems are similar to the experimental conditions for the data shown in Figures 2a,b and 4.

In relation to the PO_4 adsorption, comparing Figure 6a,b shows that the Ca-PO_4 synergy is more notorious at high pH values, in agreement with our experimental results (Figures 1 and 2). The ternary complex formation is mainly due to the formation of MPCa. The ternary complex formation reduces the contribution of the bidentate PO_4 surface complexes (B, BH) to the overall PO_4 adsorption, while the speciation of both monodentate PO_4 species (MH, MH_2) is hardly affected. A similar result is found for the PO_4 surface speciation in binary Mg-PO_4 systems (Figure S5).

Comparing Figure 6c,d shows that the Ca adsorption strongly increases in the presence of PO_4. At low pH values, Ca is mainly bound as a ternary complex in the binary Ca-PO_4 systems. In the absence of PO_4 (Figure 6c), hardly any Ca is bound at low pH. The stimulating role of PO_4 due to favorable electrostatics is mainly visible at high pH. In the presence of PO_4, more Ca is clearly bound as bidentate species (BCa), as it is evident from comparing Figure 6c,d. Especially, the Ca adsorption to the low affinity sites (BCa(l)) is enhanced at high pH conditions. The Ca binding to the high affinity sites (BCa(h)) is hardly affected, which is due to near-saturation of these sites, as observed already in the single-ion systems in the absence of PO_4.

3.4. Comparing Ferrihydrite and Goethite. The synergistic interaction of Ca with PO_4 has been studied extensively in the past for well-crystallized goethite,[34] allowing us to compare it with the interaction presently measured for Fh. In Figure 7, the PO_4 adsorption isotherms of Fh (panel a) and goethite (panel b) have been calculated for systems at pH 5 and 7 in the presence (symbols) and absence (lines) of Ca at a constant ionic strength of 3 mM. In the absence of Ca, the pH dependency of the PO_4 adsorption is much larger for Fh than for goethite, which can be attributed to more protonation of adsorbed PO_4 at low pH values.[26] In the presence of Ca, the pH dependency is much smaller for the reasons discussed below.

The intrinsic difference in the pH dependency of the PO_4 adsorption of Fh and goethite is illustrated in Figure 7a,b with model lines calculated for systems at pH 5 and 7 in $NaNO_3$ solution. This pH dependency is much higher for Fh than for goethite. At pH 7, the PO_4 adsorption in $NaNO_3$ is very similar for Fh and goethite (dotted lines). However, at pH 5 the

https://dx.doi.org/10.1021/acsearthspacechem.9b00320
ACS Earth Space Chem. XXXX, XXX, XXX−XXX

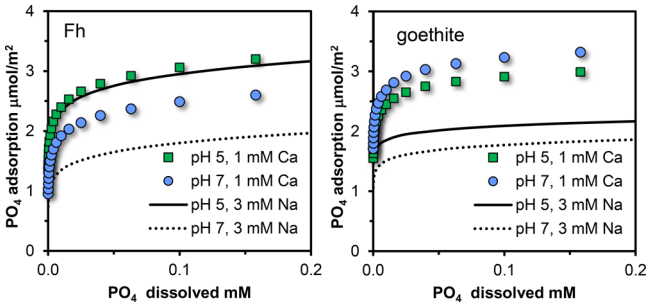

Figure 7. PO_4 adsorption isotherms of (a) ferrihydrite and (b) goethite at pH 5 and 7 in the absence (lines) and presence (symbols) of Ca at a constant ionic strength of 3 mM. The intrinsic pH dependency of the PO_4 adsorption in the $NaNO_3$ solutions is much higher for Fh than for goethite (lines). This difference is largely, though not entirely, compensated by the presence of Ca (symbols). For Fh, the PO_4 adsorption is increased by ternary Ca-PO_4 complex formation, particularly at high pH (Figure 6), and for goethite, the increase is due to a strong electrostatic interaction of adsorbed Ca^{2+} by introducing positive charge mainly to the first Stern plane, where the negatively charged outer ligands of the adsorbed PO_4 ions reside (see text). For Fh, the adsorption of PO_4 has been calculated using the parameter sets of Tables 1 and 2 and Table S4 in the Supporting Information. For goethite, the adsorption has been calculated with the parameter sets of Hiemstra et al.[43]

adsorption of PO_4 in $NaNO_3$ is much higher for Fh (full lines) than for goethite. As mentioned above, this is particularly due to a difference in protonation of the adsorbed PO_4 species.[26] For Fh (Figure 7a), the presence of Ca^{2+} hardly affects the PO_4 adsorption at pH 5 (green squares *vs* full line), although some Ca^{2+} ions do adsorb but this is mainly in the form of ternary Fe-PO_4-Ca complexes. The corresponding adsorbed Ca does not have a strong electrostatic interaction with the other types of adsorbed PO_4 ions because a significant part of the Ca charge is outside the inner Stern region according to our CD analysis (see Δz_2 in Table 2). In contrast, in the Ca-goethite, there is a substantial increase in the PO_4 adsorption at pH = 5 (Figure 7b), which is due to a strong electrostatic interaction of the adsorbed Ca^{2+} ions with adsorbed PO_4. For goethite, most of the divalent charge of Ca^{2+} is present at the 1-plane (Δz_1) and acts on the negatively charge of the outer oxygen ligands of PO_4 that reside there. This strong electrostatic interaction of Ca^{2+} also occurs at pH 7, increasing the PO_4 adsorption to similar levels as that for pH 5. For Fh at pH 7, the PO_4 adsorption is also increased in the presence of Ca^{2+} (blue circles *vs* dotted line). However, this increase is mainly due to the significant formation of ternary Ca-PO_4 complexes, and it is less important than the increase in the PO_4 adsorption on goethite by electrostatic interaction of the large fraction of Ca^{2+} charges present in the 1-plane.

The abovementioned difference in the pH-dependent adsorption behavior of PO_4 for both Fe (hydr)oxide minerals will be important in applications of surface complexation modeling in natural systems. It is evident that the choice of a proxy for the natural oxide fraction will be crucial for the outcome of predictions, particularly the pH dependency, as illustrated in Figure 7. In future applications to soils, this will be evaluated.

4. CONCLUSIONS

In this study, the surface interaction of the alkaline-earth metal ions Ca^{2+} and Mg^{2+} with adsorbed PO_4 has been quantified for well-characterized, freshly precipitated Fh. The collected data have been interpreted with the CD model in combination with a recently developed multisite ion complexation model for Fh, in which reactive site densities are based on analysis of the surface structure. In addition, high and low affinity (log *K*) sites are distinguished in the model, derived from the adsorption of alkaline-earth metal ions (M^{2+}) covering a wide range of surface loadings. The corresponding adsorption densities have been quantified in a parallel study using single-ion systems.[67] According to that study, the alkaline-earth metal ions form binuclear double-corner (^2C) inner-sphere complexes $\equiv(FeOH)_2^{\Delta z0}M^{\Delta z1}$, for which the CD coefficients have been derived with a Brown bond valence analysis using MO/DFT optimized geometries of complexes.

In the present study with binary M^{2+}-PO_4 systems, the adsorption of Ca^{2+} and Mg^{2+} ions to Fh is found to be enhanced in the presence of adsorbed PO_4 and *vice versa*. For Fh, this synergistic effect is due to the combined effect of an enhanced electrostatic interaction and the formation of ternary surface complexes. For the Ca-PO_4 systems, our model reveals the formation of two anion-bridged surface ternary complexes: $\equiv FeOPO_3Ca$ and $\equiv(FeO)_2PO_2Ca$, the former being most prominently present. The charge attribution to the surface (Δz_0) has been derived for both complexes from the MO/DFT/B3LYP/6-31+G** optimized geometries. The Ca^{2+} ion charge is distributed between the inner (Δz_1) and outer Stern (Δz_2) plane, which we found by analysis of the adsorption data with CD modeling. For the Mg-PO_4 systems, only the formation of the ternary complex $\equiv FeOPO_3Mg$ could be revealed under the investigated adsorption conditions. Our results are in line with the general notion that the dominant type of ternary complex (i.e., metal-bridged *vs* anion-bridged) depends on the relative affinity of the co-adsorbing ions for the metal (hydr)oxide surface. PO_4 has a significantly higher intrinsic affinity than Ca and Mg for binding sites at the surface of Fh, favoring the formation of anion-bridged ternary complexes. This is indeed found in our CD modeling. In addition, our modeling reveals that the distribution between monodentate and bidentate surface complexes of PO_4 is different in the single-ion and binary systems. In the presence of M^{2+}, more PO_4 is bound to Fh in a monodentate configuration compared to the single-ion systems.

The pH dependency of the intrinsic PO_4 adsorption in $NaNO_3$ solution is much larger for Fh than for goethite. However, this difference is largely compensated by the binding of Ca. For Fh, the increase in PO_4 adsorption is predominantly due to the formation of ternary Fe-PO_4-Ca surface complexes, and in the case of goethite, the increase is entirely due to a mutual electrostatic interaction of adsorbed Ca^{2+} and PO_4. From an environmental perspective, the present study is highly relevant because Ca^{2+} and Mg^{2+} ions are abundant in natural systems. The interaction of Ca^{2+} and Mg^{2+} with the surfaces of metal (hydr)oxides affects the chemical behavior and fate of other important ions, particularly anions, as shown here for PO_4. Fh can be used as a proxy for the natural oxide fraction, and application of the results of the present study will contribute to improved understanding of the mutual interactions of PO_4 and M^{2+} in soils, aquifers, and natural water bodies.

https://dx.doi.org/10.1021/acsearthspacechem.9b00320
ACS Earth Space Chem. XXXX, XXX, XXX−XXX

■ ASSOCIATED CONTENT

Supporting Information

The Supporting Information is available free of charge at https://pubs.acs.org/doi/10.1021/acsearthspacechem.9b00320.

Conditions of the batch adsorption experiments (1), thermodynamic databases used in the modeling (2), effect of phosphate adsorption on the net charge of ferrihydrite (3), precipitation of Ca-PO_4 minerals (4), charge distribution of the ternary complexes (5), modeling of Mg-PO_4 interaction with no ternary complex formation (6), surface speciation of PO_4 and Mg in ferrihydrite systems (7), and modeling PO_4 binding: Ca *vs* Mg systems (8) (PDF)

■ AUTHOR INFORMATION

Corresponding Author

Juan C. Mendez − *Soil Chemistry and Chemical Soil Quality Group, Wageningen University, 6708 PB Wageningen, The Netherlands;* orcid.org/0000-0002-1658-400X; Phone: +31 317 48 2342; Email: juan.mendezfernandez@wur.nl

Author

Tjisse Hiemstra − *Soil Chemistry and Chemical Soil Quality Group, Wageningen University, 6708 PB Wageningen, The Netherlands*

Complete contact information is available at: https://pubs.acs.org/10.1021/acsearthspacechem.9b00320

Notes

The authors declare no competing financial interest.

■ ACKNOWLEDGMENTS

The grant provided by the University of Costa Rica (UCR) to the first author is gratefully acknowledged. We thank the work of He Wei and Frank van Raffe in collecting part of the Ca-PO_4 and Mg-PO_4 adsorption data, respectively. We also thank Peter Nobels from the Chemistry and Biology Soil Laboratory (CBLB) for his attentive work regarding the ICP-OES and ICP-MS analyses.

■ REFERENCES

(1) Jambor, J. L.; Dutrizac, J. E. Occurrence and Constitution of Natural and Synthetic Ferrihydrite, a Widespread Iron Oxyhydroxide. *Chem. Rev.* **1998**, *98*, 2549−2586.

(2) Hochella, M. F., Jr.; Lower, S. K.; Maurice, P. A.; Penn, R. L.; Sahai, N.; Sparks, D. L.; Twining, B. S. Nanominerals, Mineral Nanoparticles, and Earth Systems. *Science* **2008**, *319*, 1631−1635.

(3) Qafoku, N. P. Terrestrial Nanoparticles and Their Controls on Soil-/Geo-Processes and Reactions. In *Advances in agronomy*; Academic Press, 2010; Vol. 107.

(4) Hiemstra, T. Formation, Stability, and Solubility of Metal Oxide Nanoparticles: Surface Entropy, Enthalpy, and Free Energy of Ferrihydrite. *Geochim. Cosmochim. Acta* **2015**, *158*, 179−198.

(5) Liu, J.; Zhu, R.; Xu, T.; Xu, Y.; Ge, F.; Xi, Y.; Zhu, J.; He, H. Co-Adsorption of Phosphate and Zinc(II) on the Surface of Ferrihydrite. *Chemosphere* **2016**, *144*, 1148−1155.

(6) Guo, H.; Barnard, A. S. Naturally Occurring Iron Oxide Nanoparticles: Morphology, Surface Chemistry and Environmental Stability. *J. Mater. Chem. A* **2013**, *1*, 27−42.

(7) Schwertmann, U.; Friedl, J.; Stanjek, H. From Fe(III) Ions to Ferrihydrite and Then to Hematite. *J. Colloid Interface Sci.* **1999**, *209*, 215−223.

(8) Borch, T.; Kretzschmar, R.; Kappler, A.; Van Cappellen, P.; Ginder-Vogel, M.; Voegelin, A.; Campbell, K. Biogeochemical Redox Processes and Their Impact on Contaminant Dynamics. *Environ. Sci. Technol.* **2010**, *44*, 15−23.

(9) Mejia, J.; He, S.; Yang, Y.; Ginder-Vogel, M.; Roden, E. E. Stability of Ferrihydrite−Humic Acid Coprecipitates under Iron-Reducing Conditions. *Environ. Sci. Technol.* **2018**, *52*, 13174−13183.

(10) Li, G.-X.; Chen, X.-P.; Wang, X.-N.; Chen, Z.; Bao, P. Sulfur Redox Cycling Dependent Abiotic Ferrihydrite Reduction by a *Desulfitobacterium Hafniense*. *ACS Earth Space Chem.* **2018**, *2*, 496−505.

(11) Jones, A. M.; Collins, R. N.; Waite, T. D. Redox Characterization of the Fe(II)-Catalyzed Transformation of Ferrihydrite to Goethite. *Geochim. Cosmochim. Acta* **2017**, *218*, 257−272.

(12) Burton, E. D.; Hockmann, K.; Karimian, N.; Johnston, S. G. Antimony Mobility in Reducing Environments: The Effect of Microbial Iron(III)-Reduction and Associated Secondary Mineralization. *Geochim. Cosmochim. Acta* **2019**, *245*, 278−289.

(13) Adhikari, D.; Sowers, T.; Stuckey, J. W.; Wang, X.; Sparks, D. L.; Yang, Y. Formation and Redox Reactivity of Ferrihydrite-Organic Carbon-Calcium Co-Precipitates. *Geochim. Cosmochim. Acta* **2019**, *244*, 86−98.

(14) Dzombak, D. A.; Morel, F. M. M. *Surface Complexation Modeling: Hydrous Ferric Oxide*; John Wiley & Sons, Inc.: New York, 1990.

(15) Cornell, R. M.; Schwertmann, U. *The Iron Oxides: Structure, Properties, Reactions, Ocurrence and Uses*, Second Ed.; WILEY-VCH, Germany, 2003.

(16) Hiemstra, T.; Mendez, J. C.; Li, J. Evolution of the Reactive Surface Area of Ferrihydrite: Time, PH, and Temperature Dependency of Growth by Ostwald Ripening. *Environ. Sci. Nano* **2019**, *6*, 820−833.

(17) Hiemstra, T. Surface and Mineral Structure of Ferrihydrite. *Geochim. Cosmochim. Acta* **2013**, *105*, 316−325.

(18) Davis, J. A.; Leckie, J. O. Surface Ionization and Complexation at the Oxide/Water Interface II. Surface Properties of Amorphous Iron Oxyhydroxide and Adsorption of Metal Ions. *J. Colloid Interface Sci.* **1978**, *67*, 90−107.

(19) Waite, T. D.; Davis, J. A.; Payne, T. E.; Waychunas, G. A.; Xu, N. Uranium(VI) Adsorption to Ferrihydrite: Application of a Surface Complexation Model. *Geochim. Cosmochim. Acta* **1994**, *58*, 5465−5478.

(20) Benjamin, M. M.; Leckie, J. O. Multiple-Site Adsorption of Cd, Cu, Zn, and Pb on Amorphous Iron Oxyhydroxide. *J. Colloid Interface Sci.* **1981**, *79*, 209−221.

(21) Kinniburgh, D. G.; Jackson, M. L. Concentration and PH Dependence of Calcium and Zinc Adsorption by Iron Hydrous Oxide Gel. *Soil Sci. Soc. Am. J.* **1982**, *46*, 56−61.

(22) Zachara, J. M.; Girvin, D. C.; Schmidt, R. L.; Resch, C. T. Chromate Adsorption on Amorphous Iron Oxyhydroxide in the Presence of Major Groundwater Ions. *Environ. Sci. Technol.* **1987**, *21*, 589−594.

(23) Wang, X.; Kubicki, J. D.; Boily, J.-F.; Waychunas, G. A.; Hu, Y.; Feng, X.; Zhu, M. Binding Geometries of Silicate Species on Ferrihydrite Surfaces. *ACS Earth Space Chem.* **2018**, *2*, 125−134.

(24) Johnston, C. P.; Chrysochoou, M. Mechanisms of Chromate, Selenate, and Sulfate Adsorption on Al-Substituted Ferrihydrite: Implications for Ferrihydrite Surface Structure and Reactivity. *Environ. Sci. Technol.* **2016**, *50*, 3589−3596.

(25) Tiberg, C.; Gustafsson, J. P. Phosphate Effects on Cadmium(II) Sorption to Ferrihydrite. *J. Colloid Interface Sci.* **2016**, *471*, 103−111.

(26) Hiemstra, T.; Zhao, W. Reactivity of Ferrihydrite and Ferritin in Relation to Surface Structure, Size, and Nanoparticle Formation Studied for Phosphate and Arsenate. *Environ. Sci. Nano* **2016**, *3*, 1265−1279.

(27) Mendez, J. C.; Hiemstra, T. Carbonate Adsorption to Ferrihydrite: Competitive Interaction with Phosphate for Use in Soil Systems. *ACS Earth Space Chem.* **2019**, *3*, 129−141.

(28) Liu, J.; Zhu, R.; Liang, X.; Ma, L.; Lin, X.; Zhu, J.; He, H.; Parker, S. C.; Molinari, M. Synergistic Adsorption of Cd(II) with Sulfate/Phosphate on Ferrihydrite: An in Situ ATR-FTIR/2D-COS Study. *Chem. Geol.* **2018**, *477*, 12−21.
(29) Trivedi, P.; Dyer, J. A.; Sparks, D. L. Lead Sorption onto Ferrihydrite. 1. A Macroscopic and Spectroscopic Assessment. *Environ. Sci. Technol.* **2003**, *37*, 908−914.
(30) Swedlund, P. J.; Miskelly, G. M.; McQuillan, A. J. Silicic Acid Adsorption and Oligomerization at the Ferrihydrite - Water Interface: Interpretation of ATR-IR Spectra Based on a Model Surface Structure. *Langmuir* **2010**, *26*, 3394−3401.
(31) Antelo, J.; Arce, F.; Fiol, S. Arsenate and Phosphate Adsorption on Ferrihydrite Nanoparticles. Synergetic Interaction with Calcium Ions. *Chem. Geol.* **2015**, *410*, 53−62.
(32) Bompoti, N. M.; Chrysochoou, M.; Machesky, M. L. A Unified Surface Complexation Modeling Approach for Chromate Adsorption on Iron Oxides. *Environ. Sci. Technol.* **2019**, *53*, 6352−6361.
(33) Ali, M. A.; Dzombak, D. A. Effects of Simple Organic Acids on Sorption of Cu^{2+} and Ca^{2+} on Goethite. *Geochim. Cosmochim. Acta* **1996**, *60*, 291−304.
(34) Rietra, R. P. J. J.; Hiemstra, T.; van Riemsdijk, W. H. Interaction between Calcium and Phosphate Adsorption on Goethite. *Environ. Sci. Technol.* **2001**, *35*, 3369−3374.
(35) Stachowicz, M.; Hiemstra, T.; van Riemsdijk, W. H. Multi-Competitive Interaction of As(III) and As(V) Oxyanions with Ca^{2+}, Mg^{2+}, $PO^{3-}{}_4$, and $CO^{2-}{}_3$ Ions on Goethite. *J. Colloid Interface Sci.* **2008**, *320*, 400−414.
(36) Atouei, M. T.; Rahnemaie, R.; Kalanpa, E. G.; Davoodi, M. H. Competitive Adsorption of Magnesium and Calcium with Phosphate at the Goethite Water Interface: Kinetics, Equilibrium and CD-MUSIC Modeling. *Chem. Geol.* **2016**, *437*, 19−29.
(37) Nie, Z.; Finck, N.; Heberling, F.; Pruessmann, T.; Liu, C.; Lützenkirchen, J. Adsorption of Selenium and Strontium on Goethite: EXAFS Study and Surface Complexation Modeling of the Ternary Systems. *Environ. Sci. Technol.* **2017**, *51*, 3751−3758.
(38) Likens, G. E.; Driscoll, C. T.; Buso, D. C.; Siccama, T. G.; Johnson, C. E.; Lovett, G. M.; Fahey, T. J.; Reiners, W. A.; Ryan, D. F.; Martin, C. W.; et al. The Biogeochemistry of Calcium at Hubbard Brook. *Biogeochemistry* **1998**, *41*, 89−173.
(39) Qadir, M.; Schubert, S.; Oster, J. D.; Sposito, G.; Minhas, P. S.; Cheraghi, S. A. M.; Murtaza, G.; Mirzabaev, A.; Saqib, M. High-magnesium Waters and Soils: Emerging Environmental and Food Security Constraints. *Sci. Total Environ.* **2018**, *642*, 1108−1117.
(40) Weng, L.; Vega, F. A.; van Riemsdijk, W. H. Competitive and Synergistic Effects in PH Dependent Phosphate Adsorption in Soils: LCD Modeling. *Environ. Sci. Technol.* **2011**, *45*, 8420−8428.
(41) Slomp, C. P.; Van Der Gaast, S. J.; Van Raaphorst, W. Phosphorus Binding by Poorly Crystalline Iron Oxides in North Sea Sediments. *Mar. Chem.* **1996**, *52*, 55−73.
(42) Gottselig, N.; Nischwitz, V.; Meyn, T.; Amelung, W.; Bol, R.; Halle, C.; Vereecken, H.; Siemens, J.; Klumpp, E. Phosphorus Binding to Nanoparticles and Colloids in Forest Stream Waters. *Vadose Zo. J.* **2017**, *16* (), DOI: 10.2136/vzj2016.07.0064.
(43) Hiemstra, T.; Antelo, J.; Rahnemaie, R.; van Riemsdijk, W. H. Nanoparticles in Natural Systems I: The Effective Reactive Surface Area of the Natural Oxide Fraction in Field Samples. *Geochim. Cosmochim. Acta* **2010**, *74*, 41−58.
(44) Koopmans, G. F.; Hiemstra, T.; Vaseur, C.; Chardon, W. J.; Voegelin, A.; Groenenberg, J. E. Use of Iron Oxide Nanoparticles for Immobilizing Phosphorus In-Situ: Increase in Soil Reactive Surface Area and Effect on Soluble Phosphorus. *Sci. Total Environ.* **2020**, *711*, 135220.
(45) Weng, L.; van Riemsdijk, W. H.; Hiemstra, T. Factors Controlling Phosphate Interaction with Iron Oxides. *J. Environ. Qual.* **2012**, *41*, 628−635.
(46) Schofield, R. K. Can a Precise Meaning Be given to Available Soil Phosphorus? *Soils Fert.* **1955**, *18*, 373−375.
(47) Aslyng, H. C. Phosphate Potential and Phosphate Status of Soils. *Acta Agric. Scand.* **1964**, *14*, 261−285.
(48) Koopmans, G. F.; Chardon, W. J.; Dekker, P. H. M.; Römkens, P. F. A. M.; Schoumans, O. F. Comparing Different Extraction Methods for Estimating Phosphorus Solubility in Various Soil Types. *Soil Sci.* **2006**, *171*, 103−116.
(49) Houba, V. J. G.; Temminghoff, E. J. M.; Gaikhorst, G. A.; van Vark, W. Soil Analysis Procedures Using 0.01 M Calcium Chloride as Extraction Reagent. *Commun. Soil Sci. Plant Anal.* **2000**, *31*, 1299−1396.
(50) Houba, V. J. G.; Novozamsky, I.; Huybregts, A. W. M.; van der Lee, J. J. Comparison of Soil Extractions by 0.01M $CaCl_2$, by EUF and by Some Conventional Extraction Procedures. *Plant Soil* **1986**, *96*, 433−437.
(51) Sánchez-Alcalá, I.; del Campillo, M. C.; Torrent, J. Extraction with 0.01 m $CaCl_2$ Underestimates the Concentration of Phosphorus in the Soil Solution. *Soil Use Manag.* **2014**, 297.
(52) Weesner, F. J.; Bleam, W. F. Binding Characteristics of Pb^{2+} on Anion-Modified and Pristine Hydrous Oxide Surfaces Studied by Electrophoretic Mobility and x-Ray Absorption Spectroscopy. *J. Colloid Interface Sci.* **1998**, *205*, 380−389.
(53) Elzinga, E. J.; Kretzschmar, R. In Situ ATR-FTIR Spectroscopic Analysis of the Co-Adsorption of Orthophosphate and Cd(II) onto Hematite. *Geochim. Cosmochim. Acta* **2013**, *117*, 53−64.
(54) Swedlund, P. J.; Webster, J. G.; Miskelly, G. M. The Effect of SO_4 on the Ferrihydrite Adsorption of Co, Pb and Cd: Ternary Complexes and Site Heterogeneity. *Appl. Geochem.* **2003**, *18*, 1671−1689.
(55) van Genuchten, C. M.; Gadgil, A. J.; Peña, J. Fe(III) Nucleation in the Presence of Bivalent Cations and Oxyanions Leads to Subnanoscale 7 Å Polymers. *Environ. Sci. Technol.* **2014**, *48*, 11828−11836.
(56) Wang, L.; Nancollas, G. H. Calcium Orthophosphates: Crystallization and Dissolution. *Chem. Rev.* **2008**, *108*, 4628−4669.
(57) Scheinost, A. C.; Abend, S.; Pandya, K. I.; Sparks, D. L. Kinetic Controls on Cu and Pb Sorption by Ferrihydrite. *Environ. Sci. Technol.* **2001**, *35*, 1090−1096.
(58) Greffié, C.; Amouric, M.; Parron, C. HRTEM Study of Freeze-Dried and Untreated Synthetic Ferrihydrites: Consequences of Sample Processing. *Clay Miner.* **2001**, *36*, 381−387.
(59) Mendez, J. C.; Hiemstra, T. Surface Area of Ferrihydrite Consistently Related to Primary Surface Charge, Ion Pair Formation, and Specific Ion Adsorption. *Chem. Geol.* **2020**, *532*, 119304.
(60) Thomasarrigo, L. K.; Kaegi, R.; Kretzschmar, R. Ferrihydrite Growth and Transformation in the Presence of Ferrous Iron and Model Organic Ligands. *Environ. Sci. Technol.* **2019**, *53*, 13636−13647.
(61) Lu, Y.; Hu, S.; Wang, Z.; Ding, Y.; Lu, G.; Lin, Z.; Dang, Z.; Shi, Z. Ferrihydrite Transformation under the Impact of Humic Acid and Pb: Kinetics, Nanoscale Mechanisms, and Implications for C and Pb Dynamics. *Environ. Sci. Nano* **2019**, *6*, 747−762.
(62) Hiemstra, T.; Van Riemsdijk, W. H. A Surface Structural Approach to Ion Adsorption: The Charge Distribution (CD) Model. *J. Colloid Interface Sci.* **1996**, *179*, 488−508.
(63) Hiemstra, T.; Van Riemsdijk, W. H. On the Relationship between Charge Distribution, Surface Hydration, and the Structure of the Interface of Metal Hydroxides. *J. Colloid Interface Sci.* **2006**, *301*, 1−18.
(64) Hiemstra, T.; Van Riemsdijk, W. H. A Surface Structural Model for Ferrihydrite I: Sites Related to Primary Charge, Molar Mass, and Mass Density. *Geochim. Cosmochim. Acta* **2009**, *73*, 4423−4436.
(65) Keizer, M. G.; van Riemsdijk, W. H. *ECOSAT, Equilibrium Calculation of Speciation and Transport*. Technical Report. Department of Soil Quality. Wageningen Univeristy; 1998.
(66) Kinniburgh, D. G. *Fit, Technical Report WD/93/23*; Keyworth, Great Britain, 1993.
(67) Mendez, J. C.; Hiemstra, T. High and Low Affinity Sites of Ferrihydrite for Metal Ion Adsorption: Data and Modeling of the Alkaline-Earth Ions Be, Mg, Ca, Sr, Ba, and Ra. *Geochim. Cosmochim. Acta* **2020**, Submitted.

https://dx.doi.org/10.1021/acsearthspacechem.9b00320
ACS Earth Space Chem. XXXX, XXX, XXX−XXX

(68) Brown, I. D.; Altermatt, D. Bond-Valence Parameters Obtained from a Systematic Analysis of the Inorganic Crystal Structure Database. *Acta Crystallogr., Sect. B: Struct. Sci.* **1985**, *41*, 244−247.
(69) Brown, I. D. Recent Developments in the Methods and Applications of the Bond Valence Model. *Chem. Rev.* **2009**, *109*, 6858−6919.
(70) Michel, F. M.; Ehm, L.; Antao, S. M.; Lee, P. L.; Chupas, P. J.; Liu, G.; Strongin, D. R.; Schoonen, M. A. A.; Phillips, B. L.; Parise, J. B. The Structure of Ferrihydrite, a Nanocrystalline Material. *Science* **2007**, *316*, 1726−1729.
(71) Michel, F. M.; Barron, V.; Torrent, J.; Morales, M. P.; Serna, C. J.; Boily, J.-F.; Liu, Q.; Ambrosini, A.; Cismasu, A. C.; Brown, G. E. Ordered Ferrimagnetic Form of Ferrihydrite Reveals Links among Structure, Composition, and Magnetism. *Proc. Natl. Acad. Sci. U. S. A.* **2010**, *107*, 2787−2792.
(72) Hiemstra, T. Ferrihydrite Interaction with Silicate and Competing Oxyanions: Geometry and Hydrogen Bonding of Surface Species. *Geochim. Cosmochim. Acta* **2018**, *238*, 453−476.
(73) Hiemstra, T. Surface Structure Controlling Nanoparticle Behavior: Magnetism of Ferrihydrite, Magnetite, and Maghemite. *Environ. Sci. Nano* **2018**, *5*, 752−764.
(74) Axe, L.; Bunker, G. B.; Anderson, P. R.; Tyson, T. A. An XAFS Analysis of Strontium at the Hydrous Ferric Oxide Surface. *J. Colloid Interface Sci.* **1998**, *199*, 44−52.
(75) Collins, C. R.; Sherman, D. M.; Ragnarsdöttir, K. V. The Adsorption Mechanism of Sr^{2+} on the Surface of Goethite. *Radiochim. Acta* **1998**, *81*, 201−206.
(76) Fuller, A. J.; Shaw, S.; Peacock, C. L.; Trivedi, D.; Burke, I. T. EXAFS Study of Sr Sorption to Illite, Goethite, Chlorite, and Mixed Sediment under Hyperalkaline Conditions. *Langmuir* **2016**, *32*, 2937−2946.
(77) Kinniburgh, D. G. The H^+/M^{2+} Exchange Stoichiometry of Calcium and Zinc Adsorption by Ferrihydrite. *J. Soil Sci.* **1983**, *34*, 759−768.
(78) Kinniburgh, D. G.; Barker, J. A.; Whitfield, M. A Comparison of Some Simple Adsorption Isotherms for Describing Divalent Cation Adsorption by Ferrihydrite. *J. Colloid Interface Sci.* **1983**, *95*, 370−384.
(79) Lin, J.; Zhan, Y.; Wang, H.; Chu, M.; Wang, C.; He, Y.; Wang, X. Effect of Calcium Ion on Phosphate Adsorption onto Hydrous Zirconium Oxide. *Chem. Eng. J.* **2017**, *309*, 118−129.
(80) Yao, W.; Millero, F. J. Adsorption of Phosphate on Manganese Dioxide in Seawater. *Environ. Sci. Technol.* **1996**, *30*, 536−541.
(81) Voegelin, A.; Kaegi, R.; Frommer, J.; Vantelon, D.; Hug, S. J. Effect of Phosphate, Silicate, and Ca on Fe(III)-Precipitates Formed in Aerated Fe(II)- and As(III)-Containing Water Studied by X-Ray Absorption Spectroscopy. *Geochim. Cosmochim. Acta* **2010**, *74*, 164−186.
(82) Ronson, T. K.; McQuillan, A. J. Infrared Spectroscopic Study of Calcium and Phosphate Ion Coadsorption and of Brushite Crystallization on TiO_2. *Langmuir* **2002**, *18*, 5019−5022.
(83) Daniele, P. G.; Foti, C.; Gianguzza, A.; Prenesti, E.; Sammartano, S. Weak Alkali and Alkaline Earth Metal Complexes of Low Molecular Weight Ligands in Aqueous Solution. *Coord. Chem. Rev.* 2008, 1093−1107, DOI: 10.1016/j.ccr.2007.08.005.
(84) Zhang, G. Y.; Peak, D. Studies of Cd(II)−Sulfate Interactions at the Goethite−Water Interface by ATR-FTIR Spectroscopy. *Geochim. Cosmochim. Acta* **2007**, *71*, 2158−2169.
(85) Ostergren, J. D.; Brown, G. E., Jr.; Parks, G. A.; Persson, P. Inorganic Ligand Effects on Pb(II) Sorption to Goethite (α-FeOOH) − II. Sulfate. *J. Colloid Interface Sci.* **2000**, *225*, 483−493.
(86) Tiberg, C.; Sjöstedt, C.; Persson, I.; Gustafsson, J. P. Phosphate Effects on Copper(II) and Lead(II) Sorption to Ferrihydrite. *Geochim. Cosmochim. Acta* **2013**, *120*, 140−157.

https://dx.doi.org/10.1021/acsearthspacechem.9b00320
ACS Earth Space Chem. XXXX, XXX, XXX−XXX